

Phase diagram of a non-Abelian Aubry-André-Harper model with p -wave superfluidity

Jun Wang¹, Xia-Ji Liu², Gao Xianlong¹, and Hui Hu^{1,2*}

¹*Department of Physics, Zhejiang Normal University, Jinhua 321004, China and*

²*Centre for Quantum and Optical Science, Swinburne University of Technology, Melbourne 3122, Australia*

(Dated: May 15, 2015)

We theoretically study a one-dimensional quasi-periodic Fermi system with topological p -wave superfluidity, which can be deduced from a topologically non-trivial tight-binding model on the square lattice in a uniform magnetic field and subject to a non-Abelian gauge field. The system may be regarded a non-Abelian generalization of the well-known Aubry-André-Harper model. We investigate its phase diagram as functions of the strength of the quasi-disorder and the amplitude of the p -wave order parameter, through a number of numerical investigations, including a multifractal analysis. There are four distinct phases separated by three critical lines, i.e., two phases with all extended wave-functions (I and IV), a topologically trivial phase (II) with all localized wave-functions and a critical phase (III) with all multifractal wave-functions. The phase I is related to the phase IV by duality. It also seems to be related to the phase II by duality. Our proposed phase diagram may be observable in current cold-atom experiments, in view of simulating non-Abelian gauge fields and topological insulators/superfluids with ultracold atoms.

PACS numbers: 71.23.Ft, 73.43.Nq, 67.85.-d,

I. INTRODUCTION

The Aubry-André-Harper (AAH) model is a workhorse for the study of dynamics of particles in one-dimensional (1D) quasi-periodic systems^{1,2}. Over the past few decades, it has been extensively used to theoretically understand the transport and Anderson localization properties of these interesting systems, revealing a variety of transitions between metallic (extended), critical and insulator (localized) phases^{3–13}. Most recently, the AAH model has attracted renewed attentions due to its experimental realization in photonic crystals^{14–16} and ultracold atoms^{17,18}. It has been found to play a non-trivial role to characterize emerging topological states of matter^{19–29} and the intriguing phenomenon of quantum many-body localization^{30,31}.

The AAH model can be formally derived from the reduction of a two-dimensional (2D) quantum Hall system to a 1D chain³². By taking a Landau gauge for the magnetic field with ϕ flux quanta per unit cell, the motion of an electron in a 2D rectangular lattice with tight-binding hopping strengths t_x and t_y can be described by the Hofstadter Hamiltonian ($\theta_{ij}^y = 2\pi i\phi$)³²,

$$\mathcal{H}_{2D} = \sum_{ij} \left[\hat{a}_{i+1,j}^\dagger t_x \hat{a}_{i,j} + e^{i\theta_{ij}^y} \hat{a}_{i,j+1}^\dagger t_y \hat{a}_{i,j} + \text{H.c.} \right], \quad (1)$$

which has a translational symmetry in the y -direction. As a result, the momentum of the motion along the y -axis, $k_y \subseteq [0, 2\pi)$, is well defined. Defining a reduced field operator \hat{c}_i via $\hat{a}_{i,j} = e^{-ik_y j} \hat{c}_i / \sqrt{L_y}$, where L_y is the number of sites along the y -axis, we deduce from \mathcal{H}_{2D} the AAH model,

$$\mathcal{H} = \sum_i \left[t_x \left(\hat{c}_{i+1}^\dagger \hat{c}_i + \text{H.c.} \right) + t_y V_i \hat{c}_i^\dagger \hat{c}_i \right], \quad (2)$$

where $V_i \equiv 2 \cos(2\pi i\phi + k_y)$. The localization properties of the AAH model can be easily understood from the parent Hofstadter Hamiltonian. When $t_y > t_x$, the electron prefers to hop along the y -direction and its wave-function thus becomes localized in the x -axis. In contrast, when $t_y < t_x$, the electron motion will extend over the entire x -axis. Indeed, these two cases are related by the so-called Aubry-André duality, which can be easily derived by considering two different realizations of gauge for the magnetic field². On the other hand, the topological properties of the AAH model can also be understood from the 2D Hofstadter Hamiltonian that underlies the topologically non-trivial quantum Hall phenomenon.

In this work, motivated by the recent proposals of simulating non-Abelian gauge fields^{33–35} and topological insulators/superfluids^{36,37} with ultracold atoms, we consider a generalized Hofstadter Hamiltonian, obtained by using a N -component field operator $\hat{\mathbf{a}}_{i,j} = [\hat{a}_{i,j}^{(1)}, \dots, \hat{a}_{i,j}^{(N)}]^T$ in Eq. (1) and by replacing the hopping strengths t_x and t_y with two $SU(N)$ matrices \hat{T}_x and \hat{T}_y . Taking the same reduction to a 1D chain along the x -direction (i.e., using $\hat{a}_{i,j}^{(p)} = e^{-ik_y j} \hat{c}_i^{(p)} / \sqrt{L_y}$ with $p = 1, \dots, N$), we then obtain a generalized non-Abelian AAH model,

$$\mathcal{H} = \sum_i \left[\left(\hat{\mathbf{c}}_{i+1}^\dagger \hat{T}_x \hat{\mathbf{c}}_i + \text{H.c.} \right) + V_i \hat{\mathbf{c}}_i^\dagger \hat{T}_y \hat{\mathbf{c}}_i \right], \quad (3)$$

where for simplicity we have assumed that $\hat{T}_y^\dagger = \hat{T}_y$ and have used $\hat{\mathbf{c}}_i = [\hat{c}_i^{(1)}, \dots, \hat{c}_i^{(N)}]^T$.

To be concrete, we consider the simplest non-Abelian case with two-component field operator and the $SU(N = 2)$ hopping matrices

$$\hat{T}_x = t_x \hat{\sigma}_z - i\Delta \hat{\sigma}_y \quad (4)$$

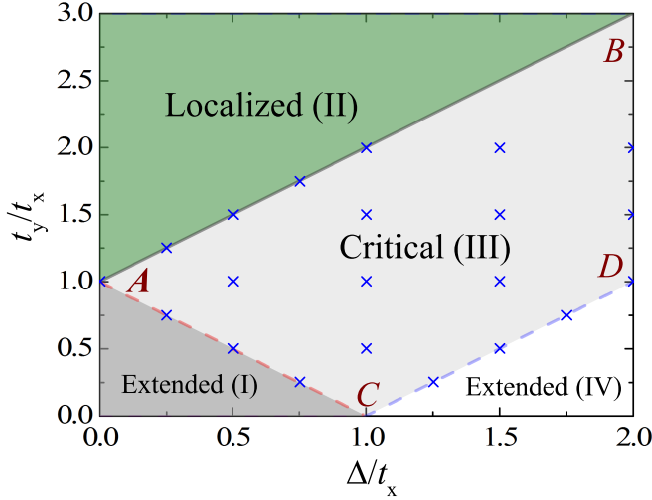


FIG. 1: (Color online). Phase diagram of a quasi-disordered Fermi system with a p -wave order parameter Δ and disorder strength t_y . The energy is in units of the hopping amplitude t_x . Four different phases are separated by the critical lines AB , AC , and CD : the phase (I) with spatially extended wave-functions, the topologically trivial phase (II) with localized wave-functions, the critical phase (III) with fractal wave-functions, and another extended phase (IV). The phases (II) and (IV) are dual to the phase (I). Multifractal analysis of wave-functions has been made for the 21 points in the critical phase (III) or on the critical lines (see Table I).

and

$$\hat{T}_y = t_y \hat{\sigma}_z, \quad (5)$$

where $\hat{\sigma}_y$ and $\hat{\sigma}_z$ are the usual 2 by 2 Pauli matrices. In the absence of the quasi-periodic disorder term (i.e., $t_y = 0$), the model describes a 1D topologically non-trivial insulator or a spinless p -wave superfluid^{38–40}. On the other hand, in the limit of $\Delta = 0$, where \hat{T}_x and \hat{T}_y commute with each other, the model reduces to the standard AAH model for each component.

We find that the localization and topological properties of the AAH model are profoundly affected by the existence of a nonzero Δ . Our main results are summarized in the phase diagram Fig. 1. There are four distinct phases (I–IV) separated by three critical lines AB , AC and CD . For a sufficiently large quasi-disorder strength, i.e., above the line AB where $t_y > t_x + \Delta$ the system becomes localized and topologically trivial^{21,22}. Below the line AC or its duality line CD , where $t_y < |t_x - \Delta|$, all the wave-functions of the system are extended. The area enclosed by the three separation lines is critical and all the wave-functions are multifractal. In this study, the phase diagram Fig. 1 is theoretically analyzed by a number of numerical approaches, including a multifractal analysis for the critical area.

The rest of the paper is organized as follows. In the next section (Sec. II), we explicitly write down the Schrödinger equation of our 1D quasi-periodic system and highlight its particle-hole symmetry and duality. In

Sec. III, we determine the phase diagram by calculating the inverse participation ratio at a given level of rational approximations and verifying single-particle wave-functions in different phases. In Sec. IV, we introduce the multifractal approach and present a scaling analysis of the structure of wave-functions in the critical regime. In Sec. V, we discuss the behavior of edge modes or Majorana fermions in different states. Section VI is devoted to conclusions and outlooks.

II. NON-ABELIAN SU(2) AUBRY-ANDRÉ-HARPER MODEL

For the non-Abelian AAH model with the hopping matrices in Eqs. (4) and (5), we may write the wave-function

$$|\psi\rangle = \sum_i \left[u_i \hat{c}_i^{(1)\dagger} + v_i \hat{c}_i^{(2)\dagger} \right] |0\rangle, \quad (6)$$

then the Schrödinger equation $\mathcal{H}|\psi\rangle = \epsilon|\psi\rangle$ has the explicit form,

$$t_x(u_{i+1} + u_{i-1}) + t_y V_i u_i - \Delta(v_{i+1} - v_{i-1}) = \epsilon u_i, \quad (7)$$

$$\Delta(u_{i+1} - u_{i-1}) - t_x(v_{i+1} + v_{i-1}) - t_y V_i v_i = \epsilon v_i. \quad (8)$$

Recall that $V_i = 2\cos(2\pi i\phi + k_y)$. Following the standard routine for investigating localization properties of the AAH model, throughout the paper we set $k_y = 0$ and take an irrational value $\phi = (\sqrt{5} - 1)/2$. This inverse of the golden mean may be approached by using the Fibonacci numbers F_n : $\phi = \lim_{n \rightarrow \infty} F_{n-1}/F_n$, where F_n is recursively defined by the relation $F_{n+1} = F_n + F_{n-1}$, with $F_0 = F_1 = 1$. Thus, in numerical calculations we take the rational approximation

$$\phi \simeq \phi_n = \frac{F_{n-1}}{F_n}. \quad (9)$$

To minimize the effect of the periodic boundary condition, we assume that the length of the system is periodic with period F_n .

At the n -th rational approximation, the Schrödinger equation then becomes periodic with period F_n . According to Bloch's theorem, the wave-function ψ can be characterized by a crystal momentum $q_x \subseteq [-\pi/F_n, +\pi/F_n]$ and satisfies $\psi_{i+F_n} = e^{iq_x F_n} \psi_i$ ($i = 0, 1, \dots, F_n - 1$). Therefore, if we represent ψ as a vector,

$$\psi = [u_0, v_0, u_1, v_1, \dots, u_{F_n-1}, v_{F_n-1}]^T, \quad (10)$$

the Schrödinger equation can be solved by finding the eigenvalues and eigenvectors of a $2F_n \times 2F_n$ matrix:

$$\mathcal{H}_n = \begin{pmatrix} A_0 & B & 0 & \dots & 0 & C \\ B^\dagger & A_1 & B & 0 & \dots & 0 \\ 0 & B^\dagger & A_2 & B & 0 & \dots & 0 \\ \vdots & \ddots & \ddots & \ddots & \ddots & \ddots & \vdots \\ 0 & \dots & 0 & B^\dagger & A_{F_n-3} & B & 0 \\ 0 & \dots & 0 & B^\dagger & A_{F_n-2} & B \\ C^\dagger & \dots & 0 & B^\dagger & A_{F_n-1} \end{pmatrix}, \quad (11)$$

where

$$A_i = 2t_y \cos(2\pi i\phi_n) \begin{pmatrix} 1 & 0 \\ 0 & -1 \end{pmatrix}, \quad (12)$$

$$B = \begin{pmatrix} t_x & -\Delta \\ \Delta & -t_x \end{pmatrix}, \quad (13)$$

and

$$C = \begin{pmatrix} t_x & \Delta \\ -\Delta & -t_x \end{pmatrix} \exp(-iq_x F_n). \quad (14)$$

The energy spectrum consists of $2F_n$ bands, each of which is a function of the crystal momentum q_x . Without loss of generality, we consider only one state in each band by taking $q_x = 0$. Numerically, we solve the eigenvalue and eigenvector problem of the matrix Eq. (11) at a given value of n and then perform a scaling analysis with increasing n . The irrational limit is reached when we extrapolate our numerical results to the scaling limit $1/n \rightarrow 0$.

A. Particle-hole symmetry

With our specific choice of SU(2) hopping matrices, the non-Abelian AAH model has an interesting particle-hole symmetry. That is, the model is invariant under the particle-hole transformation:

$$\hat{c}_i^{(1)} \leftrightarrow \hat{c}_i^{(2)\dagger}. \quad (15)$$

In other words, for every particle-like solution (u_i, v_i) of the Schrödinger Eqs. (7) and (8) with energy $E \geq 0$, there is always a hole-like solution (v_i^*, u_i^*) with energy $-E$. To highlight this particle-hole symmetry, it is useful to interpret the two components of the system as the particle and hole components of a spinless p -wave Fermi superfluid, in which the parameter Δ can be conveniently identified as a p -wave order parameter. This interpretation becomes apparent, if we set $\hat{c}_i^{(1)} = \hat{c}_i$ and $\hat{c}_i^{(2)} = \hat{c}_i^\dagger$ in the non-Abelian AAH model. It leads to a Hamiltonian that describes a 1D p -wave superfluid in a quasi-periodic potential,

$$\mathcal{H} = \sum_i \left[\left(t_x \hat{c}_{i+1}^\dagger \hat{c}_i + \Delta \hat{c}_{i+1} \hat{c}_i + \text{H.c.} \right) + t_y V_i \hat{c}_i^\dagger \hat{c}_i \right], \quad (16)$$

which shares the same energy spectrum as the AAH model. The Anderson localization of the Hamiltonian Eq. (16) has been recently analyzed by Lang *et al.*¹⁹ and DeGottardi *et al.*²¹. It was shown that the system becomes localized once $t_y > t_x + \Delta$.

B. Duality

Our non-Abelian AAH model has an interesting duality, which is very useful to understand the phase diagram.

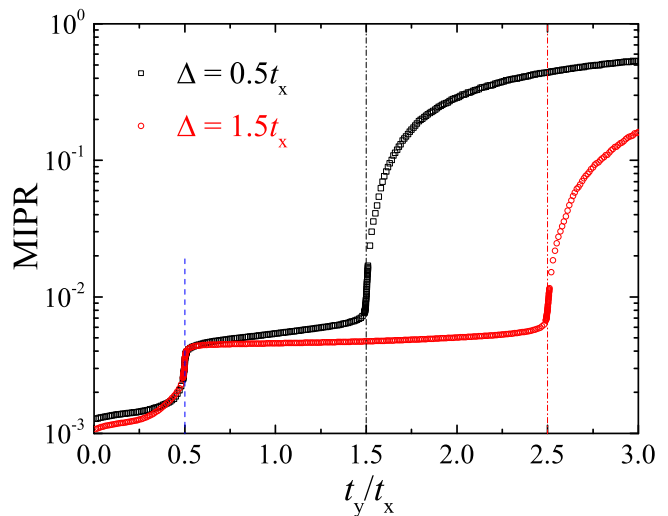


FIG. 2: (Color online) Mean inverse participation ratio (MIPR) as a function of the quasi-disorder strength at two p -wave superfluid order parameter $\Delta = 0.5t_x$ (black squares) and $\Delta = 1.5t_x$ (red circles). The dashed line and dot-dashed lines show the sharp increase of MIPR at phase boundaries. Here, we use $n = 15$ and $F_n = 987$.

In the p -wave Hamiltonian Eq. (16), if we make the following replacement for the field operator,

$$\hat{c}_i \rightarrow -\hat{d}_i^\dagger \quad \text{if } i \text{ is odd} \quad (17)$$

and

$$\hat{c}_i \rightarrow \hat{d}_i \quad \text{if } i \text{ is even}, \quad (18)$$

and replace ϕ by $\phi + 1/2$ in the quasi-periodic potential V_i , Eq. (16) keeps the same form, except that t_x and Δ are exchanged. Thus, the system is self-dual if $t_x = \Delta$.

In the absence of the p -wave order parameter ($\Delta = 0$), the AAH model also has Aubry-André duality, which relates a wave-function at $\lambda \equiv t_y/t_x = a$ to the one at $\lambda = 1/a$ by a Fourier transformation². From the phase diagram Fig. 1, a similar duality seems to exist if $\Delta \neq 0$. Unfortunately, we are not able to find a simple transformation to relate the parameters t_x and t_y for a given Δ , or the parameters Δ and t_y for a given t_x .

III. INVERSE PARTICIPATION RATIO AND PHASE DIAGRAM

A useful quantity in characterizing phase transitions of quasi-periodic systems is the inverse participation ratio (IPR). For a given normalized wave-function ψ , it is given by $\sum_i \psi_i^4 = \sum_i [u_i^4 + v_i^4]$, which measures the inverse of the number of lattice sites being occupied by particles. As we shall see, the non-Abelian AAH model considered in this work has a *pure* energy spectrum so that extended, critical and localized wave functions do

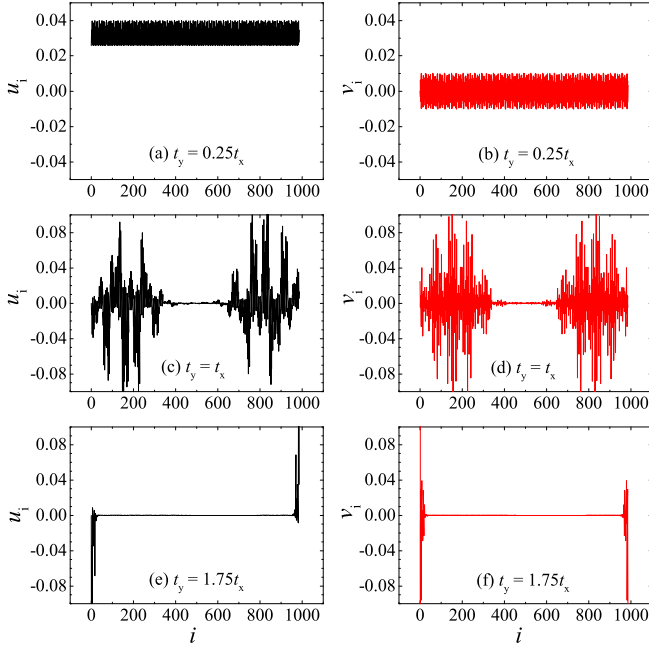


FIG. 3: (Color online) The Bogoliubov quasi-particle wave-functions of the lowest edge mode, u_i (left panel) and v_i (right panel), at the p -wave superfluid order parameter $\Delta = 0.5t_x$. From top to bottom, the strength of the quasi-disorder t_y increases from $0.25t_x$ (a, b) to t_x (c, d), and finally to $1.75t_x$ (e, f), corresponding to the cases of extended, critical and localized wave-functions, respectively. Here, we take $n = 15$ and $F_n = 987$.

not coexist (i.e., there are no mobility edges). Therefore, at the n -th rational approximation it is convenient to define a mean inverse participation ratio (MIPR),

$$\text{MIPR} = \frac{1}{2F_n} \sum_{i_E=0}^{2F_n-1} \sum_{i=0}^{F_n-1} [u_{i,i_E}^4 + v_{i,i_E}^4], \quad (19)$$

where i_E is the index of energy levels. For extended states, MIPR scales like F_n^{-1} ; while for localized states, MIPR tends to a finite value $O(1)$. For critical states, MIPR behaves like $F_n^{-\alpha}$, where $0 < \alpha < 1$ depends on the multifractal structure of wave-functions. We use MIPR to determine the phase boundaries separating the extended, critical and localized phases, which are identified by the turning points of MIPR as a function of t_y/t_x .

Figure 2 reports the evolution of MIPR in a logarithmic scale at two p -wave order parameters $\Delta = 0.5t_x$ and $\Delta = 1.5t_x$. We have used $n = 15$ and $F_n = 987$. There are two turning points of MIPR located respectively at $t_y = |t_x - \Delta|$ and $t_x + \Delta$, at which MIPR increases very rapidly. We have checked that with increasing n , the slope of MIPR at these turning points becomes sharper. Thus, we anticipate that finally there will be a jump at the turning points in the scaling limit $n \rightarrow \infty$, signaling a phase transition. The determination of the turning points of MIPR at different p -wave order parameters

leads to the proposed phase diagram shown in Fig. 1.

We find four phases (I-IV) that are separated by three critical lines AB , AC and CD . Both phases I and IV have extended wave-functions and are related to each other by the dual transformation given in Eqs. (17) and (18). All the wave-functions in the phase II are instead localized. It seems that these localized wave-functions may also relate to the extended wave-functions in the phase I (or IV) by a duality that is analogous to the Aubry-André duality occurring at $\Delta = 0$. Yet, such a duality transformation is still to be determined. The three separating lines enclose a large area in which all the wave-functions are critical.

In Fig. 3, we examine the representative ground-state wave-functions (i.e., of the state at the edge of the energy spectrum) in different phases with $\Delta = 0.5t_x$. With increasing strength of the quasi-disorder potential t_y/t_x , it is clear that the wave-function is extended in the phase I (see a and b), critical in the phase III (c and d), and localized in the phase II (e and f).

IV. MULTIFRACTAL ANALYSIS OF CRITICAL WAVE-FUNCTIONS

To strengthen the proposed phase diagram in Fig. 1, we further investigate the scaling behavior of wave-functions by using a multifractal analysis^{3,8}. At the n -th level of rational approximations, where the period of the lattice is F_n , we analyze the probability measure at the lattice site i , $p_i = u_i^2 + v_i^2$ ($i = 0, \dots, F_n - 1$), from a selected wave-function ψ , which is normalized to unity $\sum_i p_i = 1$. The scaling index α_i for p_i is defined by

$$p_i = F_n^{-\alpha_i}. \quad (20)$$

The key observable to characterize the scaling behavior of the wave-function is the singular spectrum $f_n(\alpha)$ defined by

$$\Omega_n(\alpha) = F_n^{f_n(\alpha)}, \quad (21)$$

where $\Omega_n(\alpha)d\alpha$ is the number of lattice sites, which have an index α_i distributed between α and $\alpha + d\alpha$. The singular spectrum in the scaling limit $f(\alpha)$ can be calculated as $f(\alpha) = \lim_{n \rightarrow \infty} f_n(\alpha)$. For extended wave-functions, all the lattice sites have a probability measure $p_i \sim 1/F_n$; thus $f(\alpha)$ is only defined at $\alpha = 1$ with $f(\alpha) = 1$. For localized wave-functions, on the other hand, p_i is nonzero only on a finite number of lattice sites. These sites have an index $\alpha = 0$ and the remaining sites with exponentially small probability measure have $\alpha = \infty$; thus $f(\alpha)$ takes only two values: $f(\alpha = 0) = 0$ and $f(\alpha = \infty) = 1$. For critical wave-functions, the index α has a distribution and hence the singular spectrum $f(\alpha)$ is a smooth function defined on a finite interval $[\alpha_{\min}, \alpha_{\max}]$. Therefore, it is clear that, to identify extended, critical and localized wave-function, we may simply examine the minimum value of the index α , which should take $\alpha_{\min} = 1$

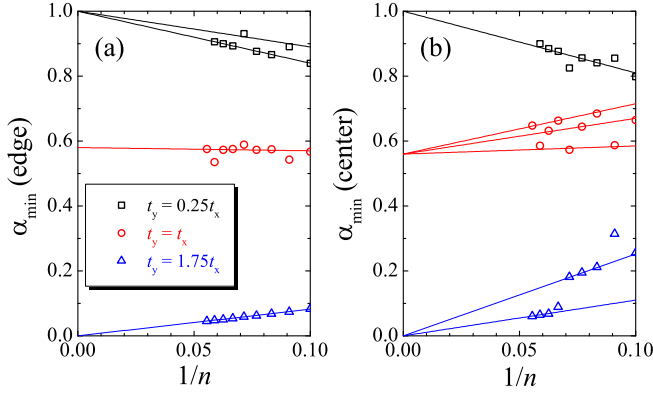


FIG. 4: (Color online) Plots of α_{\min} vs $1/n$ for the wave-functions of the lowest edge mode ($i_E = 0$) (a) and of the center mode ($i_E = F_n$) (b), at the p -wave superfluid order parameter $\Delta = 0.5t_x$. The black squares, red circles and blue triangles show the results with increasing quasi-disorder strength t_y , as indicated in the left panel (a).

(extended), $1 > \alpha_{\min} > 0$ (critical) and $\alpha_{\min} = 0$ (localized), respectively.

For the numerical calculation of $f(\alpha)$, we follow the work by Hiramoto and Kohmoto⁸ and define an entropy function,

$$\mathcal{S}_n(\alpha) = \frac{1}{n} \ln \Omega_n(\alpha), \quad (22)$$

which is related to the singular spectrum as (cf. Eq. (21))

$$f_n(\alpha) = \frac{1}{\varepsilon} \mathcal{S}_n(\alpha), \quad (23)$$

where $\varepsilon = \ln[(\sqrt{5} + 1)/2]$. The entropy function can be calculated by an analogous formalism to the usual statistical mechanics⁸. First, one introduces a partition function,

$$\mathcal{Z}_n(q) = \sum_{i=0}^{F_n-1} p_i^q,$$

and a free energy,

$$\mathcal{G}_n(q) = \frac{1}{n} \ln \mathcal{Z}_n(q). \quad (24)$$

The entropy function is then obtained through the Legendre transformation,

$$\mathcal{S}_n(\alpha) = \mathcal{G}_n(q) + q\alpha\varepsilon$$

and

$$\alpha = -\frac{1}{\varepsilon} \frac{d\mathcal{G}_n(q)}{dq}. \quad (25)$$

We have calculated $f_n(\alpha) = \mathcal{S}_n(\alpha)/\varepsilon$ for finite Fibonacci indices n and have tried to extrapolate them to

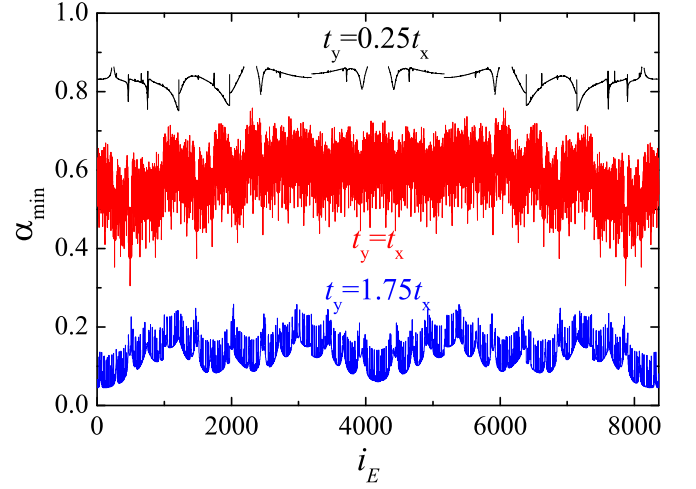


FIG. 5: (Color online) Plots of α_{\min} for the wave-function of each mode at $\Delta = 0.5t_x$ and at three different quasi-disorder strengths ($t_y/t_x = 0.25, 1$ and 1.75 from top to bottom). We have used $n = 18$ and $F_n = 4181$, so the index of energy mode i_E runs from 1 to $2F_n = 8362$.

the scaling limit $1/n \rightarrow 0$. In Fig. 4, we present examples of determining α_{\min} for wave-functions in the phases I, III and II at the p -wave order parameter $\Delta = 0.5t_x$. We consider two typical wave-functions, one at the edge of the energy spectrum (denoted by an energy index $i_E = 0$) and another at the center of the spectrum ($i_E = F_n$). For both wave-functions, α_{\min} extrapolates to 1 if $t_y = 0.25t_x$, to about 0.58 if $t_y = t_x$, and to 0 if $t_y = 1.75t_x$. In Fig. 5, we examine the value of α_{\min} for all the wave-functions at the $n = 18$ th rational approximation. For all three disorder strengths, α_{\min} varies smoothly with increasing spectrum index i_E , suggesting that there is no mobility edge in the energy spectrum. In this way, we confirm that all the wave-functions are extended in the phase I, critical in the phase III, and localized in the phase II.

We now focus on the wave-functions in the critical phase II and on the three critical lines. Table I summarizes the values of α_{\min} 's for the edge and the center of the energy spectrum for various points in the phase diagram, Fig. 1. At the duality point A of the original AAH model ($\Delta = 0$, $t_y = t_x$), our results of $\alpha_{\min}(\text{edge}) \simeq 0.17$ and $\alpha_{\min}(\text{center}) \simeq 0.36$ are consistent with the previous calculations by Hiramoto and Kohmoto⁸. Quite generally, all the edge states on an individual critical line, either AB , AC or CD (excluding the connecting points A and C), seem to have identical values of α_{\min} . This is also true for the center states, although their values of α_{\min} may be different from those of the edge states. On the other hand, all the states in the whole region III, no matter at the edge or at the center of the spectrum, have identical values of $\alpha_{\min} \simeq 0.58$. Therefore, points on an individual critical line (excluding the points A and C) or in the whole area III may belong to the same universal-ity class. Further numerical verification of this conjecture

TABLE I: Values of α_{\min} for the wave-functions at the edge and the center of the energy spectrum. The mark \times means that there is no enough convergence in data for determining α_{\min} .

Δ/t_x	t_y/t_x	position	$\alpha_{\min}(\text{edge})$	$\alpha_{\min}(\text{center})$
0	1.0	A	0.17	0.36
0.25	1.25	AB	\times	0.38
0.5	1.5	AB	\times	0.39
0.75	1.75	AB	\times	0.38
1.0	2.0	AB	\times	0.39
0.25	0.75	AC	0.58	0.67
0.5	0.5	AC	0.56	0.65
0.75	0.25	AC	0.59	0.65
1.25	0.25	CD	0.65	0.58
1.5	0.5	CD	0.64	0.59
1.75	0.75	CD	0.66	0.59
2.0	1.0	CD	0.64	0.59
0.5	1.0	III	0.58	0.56
1.0	0.5	III	0.57	0.57
1.0	1.0	III	0.57	0.56
1.0	1.5	III	0.57	0.57
1.5	1.0	III	0.57	0.58
1.5	1.5	III	0.58	0.58
1.5	2.0	III	0.57	0.58
2.0	1.5	III	0.58	0.57
2.0	2.0	III	0.57	0.57

requires the comparison of the curve $f(\alpha)$ on the whole interval $[\alpha_{\min}, \alpha_{\max}]$. Unfortunately, the convergence of our numerical estimates for $f(\alpha)$ at arbitrary α is too poor to reach a conclusive confirmation.

V. MAJORANA EDGE MODES

In the absence of the quasi-periodic potential ($t_y = 0$), the Schrödinger equations (7) and (8) hosts zero-energy edge mode at the two boundaries, as a result of its non-trivial topology in the energy band structure. These zero-energy edge modes, also referred to as Majorana fermions in the case of superfluidity, have been shown to persist at nonzero t_y , until the localized phase is reached^{21,22}. We have calculated the energy of the Majorana edge mode for a finite length system, ϵ_M , by using the open boundary condition, i.e., setting the 2×2 matrix $C = 0$ in Eq. (11).

In Fig. 6, we report the energy gap $E_{\text{gap}} = 2\epsilon_M$ as a function the system length $L = F_n$ at $\Delta = 0.5t_x$ and several quasi-disorder strengths. The length dependence of the edge-mode energy is dramatically affected by the quasi-disorder strength. For small disorder strengths in the extended phase I or the critical phase III, the energy decreases exponentially as the length of the system L increases. On the other hand, on the separating critical

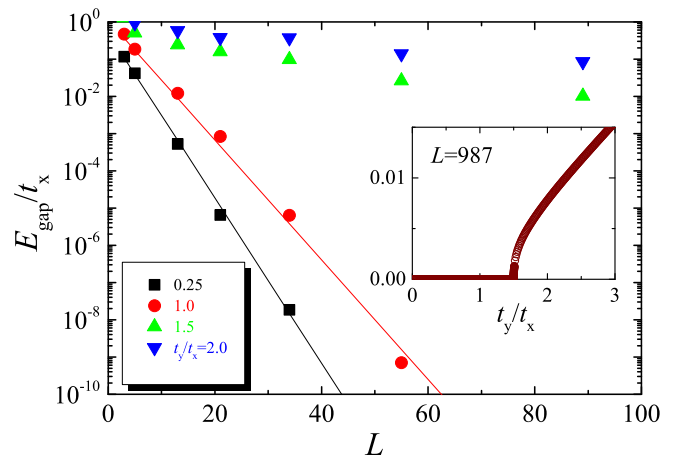


FIG. 6: (Color online) Length dependence of the energy gap at $\Delta = 0.5t_x$ and at different quasi-disorder strengths (as indicated). In the extended and critical phases, the energy gap vanishes exponentially with increasing system size, as suggested by the two exponential fitting lines. The inset shows the evolution of the energy gap with increasing quasi-disorder strength at $L = F_n = 987$, where $n = 15$. The energy gap increases rapidly after entering the localized phase (II).

line AB or in the localized phase II, the energy decreases much slower with increasing length L . At a sufficiently large length $L = F_{15} = 987$, as shown in the inset of the figure, we find that the system opens a nonzero energy gap only at the critical line AB, where $t_y > t_x + \Delta$, in consistent with previous theoretical findings^{21,22}.

VI. CONCLUSIONS

In summary, we have proposed a generalization of the Aubry-André-Harper model to the non-Abelian class with $SU(N)$ hopping matrices. The localization and topological properties of the model is greatly affected by such a generalization. We have performed a systematic investigation of the simplest $SU(2)$ case with non-trivial p -wave superfluidity and have shown that its phase diagram becomes much richer. There is a large window for the critical phase in the phase diagram, which is separated from the extended and localized phases by three critical lines. Our multifractal analysis of the critical wave-functions indicates that points on an individual critical line or in the critical phase may belong to the same universal class. Further issues - such as the spectral statistics on the critical lines and in the critical phase - are of interest and will be addressed elsewhere.

The proposed non-Abelian $SU(2)$ Aubry-André-Harper model might be realized in cold-atom laboratories in the near future. In particular, in view of recent numerous attempts for creating non-Abelian gauge fields with ultracold atoms, various non-Abelian Aubry-André-Harper models could be simulated. We anticipate even richer phase diagrams with, for example, non-pure en-

ergy spectrum, in which the extended, critical and localized states may coexist and be separated by some mobility edges. Experimentally, it would be interesting to observe mobility edges in one-dimensional quasi-periodic systems⁴¹.

Acknowledgments

XJL and HH were supported by the ARC Discovery Projects (Grant Nos. FT130100815, DP140103231,

FT140100003, and DP140100637) and NFRP-China (Grant No. 2011CB921502). GX was supported by the NSF of China (Grant Nos. 11374266 and 11174253), the Zhejiang Provincial Natural Science Foundation (Grant No. R6110175) and the Program for New Century Excellent Talents in University.

-
- * Electronic address: hhu@swin.edu.au
- ¹ P. G. Harper, Proc. Phys. Soc., London, Sect. A **68**, 874 (1955).
 - ² S. Aubry and G. André, Ann. Israel Phys. Soc. **3**, 133 (1980).
 - ³ For a review, see, for example, H. Hiramoto and M. Kohmoto, Int. J. Mod. Phys. B **06**, 281 (1992).
 - ⁴ M. Kohmoto, L. P. Kadanoff, and C. Tang, Phys. Rev. Lett. **50**, 1870 (1983).
 - ⁵ S. Ostlund, R. Pandit, D. Rand, H. J. Schellnhuber, and E. D. Siggia, Phys. Rev. Lett. **50**, 1873 (1983).
 - ⁶ M. Kohmoto, Phys. Rev. Lett. **51**, 1198 (1983).
 - ⁷ D. J. Thouless, Phys. Rev. B **28**, 4272 (1983).
 - ⁸ H. Hiramoto, M. Kohmoto, Phys. Rev. B **40**, 8225 (1989).
 - ⁹ T. Geisel, R. Ketzmerick, and G. Petschel, Phys. Rev. Lett. **66**, 1651 (1991).
 - ¹⁰ J. H. Han, D. J. Thouless, H. Hiramoto, and M. Kohmoto, Phys. Rev. B **50**, 11365 (1994).
 - ¹¹ I. Chang, K. Ikezawa, and M. Kohmoto, Phys. Rev. B **55**, 12971 (1997).
 - ¹² Y. Takada, K. Ino, and M. Yamanaka, Phys. Rev. E **70**, 066203 (2004).
 - ¹³ F. Liu, S. Ghosh, and Y. D. Chong, Phys. Rev. B **91**, 014108 (2015).
 - ¹⁴ L. Dal Negro, C. J. Oton, Z. Gaburro, L. Pavesi, P. Johnson, A. Lagendijk, R. Righini, M. Colocci, and D. S. Wiersma, Phys. Rev. Lett. **90**, 055501 (2003).
 - ¹⁵ Y. Lahini, R. Pugatch, F. Pozzi, M. Sorel, R. Morandotti, N. Davidson, and Y. Silberberg, Phys. Rev. Lett. **103**, 013901 (2009).
 - ¹⁶ Y. E. Kraus, Y. Lahini, Z. Ringel, M. Verbin, and O. Zilberberg, Phys. Rev. Lett. **109**, 106402 (2012).
 - ¹⁷ G. Roati, C. D'Errico, L. Fallani, M. Fattori, C. Fort, M. Zaccanti, G. Modugno, M. Modugno, and M. Inguscio, Nature (London) **453**, 895 (2008).
 - ¹⁸ G. Modugno, Rep. Prog. Phys. **73**, 102401 (2010).
 - ¹⁹ L.-J. Lang, X. Cai, and S. Chen, Phys. Rev. Lett. **108**, 220401 (2012).
 - ²⁰ L.-J. Lang and S. Chen, Phys. Rev. B **86**, 205135 (2012).
 - ²¹ W. DeGottardi, D. Sen, and S. Vishveshwara, Phys. Rev. Lett. **110**, 146404 (2013).
 - ²² X. Cai, L.-J. Lang, S. Chen, and Y. Wang, Phys. Rev. Lett. **110**, 176403 (2013).
 - ²³ S. Ganeshan, K. Sun, S. Das Sarma, Phys. Rev. Lett. **110**, 180403 (2013).
 - ²⁴ I. I. Satija and G. G. Naumis, Phys. Rev. B **88**, 054204 (2013).
 - ²⁵ Y. E. Kraus, and O. Zilberberg, Phys. Rev. Lett. **109**, 116404 (2013).
 - ²⁶ S.-L. Zhu, Z.-D. Wang, Y.-H. Chan, and L.-M. Duan, Phys. Rev. Lett. **110**, 075303 (2013).
 - ²⁷ F. Grusdt, M. Honing, and M. Fleischhauer, Phys. Rev. Lett. **110**, 260405 (2013).
 - ²⁸ R. Barnett, Phys. Rev. A **88**, 063631 (2013).
 - ²⁹ X. Deng and L. Santos, Phys. Rev. A **89**, 033632 (2014).
 - ³⁰ S. Iyer, V. Oganessian, G. Refael, and D. A. Huse, Phys. Rev. B **87**, 134202 (2013).
 - ³¹ M. Schreiber, S. S. Hodgman, P. Bordia, H. P. Lüschen, M. H. Fischer, R. Vosk, E. Altman, U. Schneider, and I. Bloch, arXiv:1501.05661 (unpublished).
 - ³² D. R. Hofstadter, Phys. Rev. B **14**, 2239 (1976).
 - ³³ K. Osterloh, M. Baig, L. Santos, P. Zoller, and M. Lewenstein, Phys. Rev. Lett. **95**, 010403 (2005).
 - ³⁴ N. Goldman, A. Kubasiak, P. Gaspard, and M. Lewenstein, Phys. Rev. A **79**, 023624 (2009).
 - ³⁵ N. Goldman, G. Juzeliūnas, P. Öhberg, and I. B. Spielman, Rep. Prog. Phys. **77**, 126401 (2014).
 - ³⁶ X.-J. Liu, L. Jiang, H. Pu, and H. Hu, Phys. Rev. A **85**, 021603(R) (2012).
 - ³⁷ X.-J. Liu and H. Hu, Phys. Rev. A **85**, 033622 (2012).
 - ³⁸ M. Z. Hasan and C. L. Kane, Rev. Mod. Phys. **82**, 3045 (2010).
 - ³⁹ X.-L. Qi and S.-C. Zhang, Rev. Mod. Phys. **83**, 1057 (2011).
 - ⁴⁰ S. Q. Shen, *Topological insulators* (Springer, Berlin, 2012).
 - ⁴¹ S. Ganeshan and S. Das Sarma, arXiv: 1411.7375 (unpublished).